

OpenStreetMap-based Autonomous Navigation With LiDAR Naive-Valley-Path Obstacle Avoidance [★]

Miguel Ángel Muñoz-Bañón^{a,*}, Edison Velasco-Sánchez^a, Francisco A. Candelas^a, Fernando Torres^a

^aThe authors are with the Group of Automation, Robotics and Computer Vision (AUROVA), San Vicente del Raspeig S/N, Alicante, 03009, Spain

Abstract

In this paper, we present a complete autonomous navigation pipeline for unstructured outdoor environments. The main contribution of this work is on the path planning module, which we divided into two main categories: Global Path Planning (GPP) and Local Path Planning (LPP). For environment representation, instead of complex and heavy grid maps, the GPP layer uses road network information obtained directly from OpenStreetMaps (OSM). In the LPP layer, we use a novel Naive-Valley-Path (NVP) method to generate a local path avoiding obstacles in the road in real-time. This approach uses a naive representation of the local environment using a LiDAR sensor. Also, it uses a naive optimization that exploits the concept of "valley" areas in the cost map. We demonstrate the system's robustness experimentally in our research platform BLUE, driving autonomously across the University of Alicante Scientific Park for more than 20 km in a 12.33 ha area.

Keywords:

Autonomous navigation, Robot navigation, Path planning, Obstacle avoidance, Lidar point cloud

1. Introduction

One of the most important autonomous navigation tasks is to reach a certain target given the vehicle's current pose. During this process, the vehicle is subject to constraints such as not colliding with any obstacle. This is a non-trivial task because the environment in which the vehicle navigates is usually complex, with many obstacles, and it requires the estimation of sequential intermediate goals. These goals are usually known as path. The process is widely named in the literature as path planning, and it is a multi-layer task that requires: knowledge of the environment to plan the best possible path [1, 2], scene understanding to avoid obstacles during navigation [3, 4], and generation of the control actions to fit the vehicle trajectory to the desired path [5]. Path Planning can be divided into two different categories [6, 7]: Global Path Planning (GPP) and Local Path Planning (LPP).

Global Path Planning (GPP) uses the global environmental representation to check possible paths to obtain

the best one in terms of a cost function. In this case, the environment representation usually contains persistent static elements. For this reason, the calculated path will not be strictly the one the robot will follow because the non-persistent static obstacles¹ and dynamic obstacles will force the robot to re-plan the route. GPP techniques can be classified into the graph search algorithm [8, 9], the random sampling algorithm [10, 11], and the intelligent bionic algorithm [12]. There are different classical graph search approaches in the literature, such as the Dijkstra algorithm [13], A* algorithm [14], DFS algorithm [15], and BFS algorithm [16]. In [17, 18], the authors improve the efficiency of classical graph search algorithms through a heuristic estimation, which reduces the number of searching grids and improves the searching efficiency. In most works, such as [19, 20, 21], the authors use grid maps as global environment representation. This representation is usually used in indoor applications, where the environment is highly structured and

through the grant ACIF/2019/088.

^{*}Corresponding author

Email address: miguelangel.munoz@ua.es (Miguel Ángel Muñoz-Bañón)

¹We consider non-persistent static obstacles, the static ones during the current navigation but can appear or disappear in different navigation sessions, e.g., parked cars.

[★]This work has been supported by the Spanish Government through the FPI grant PRE2019-088069 and the research project RTI2018-094279-B-I00, as well as by the regional Valencian Community Government and the European Regional Development Fund (ERDF)

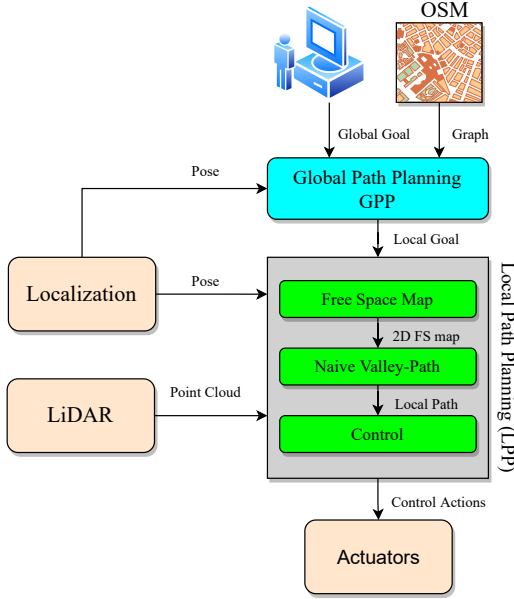


Figure 1: The complete autonomous navigation pipeline, where Path Planning approach is organized hierarchically. First, the GPP gets information about global localization from the robot and global information about the environment from OSM to plan a global path. Then, the LPP module, using the presented Naive Valley-Path method, recalculates the local path to obtain the optimal way to follow.

the size of the area is limited. However, grid maps building is not trivial in outdoor environments and has some limitations like space and global consistency. To avoid this limitations in outdoors applications, other works use available environment representation from the internet, such as top-view images [22] or OpenStreetMaps (OSM) information [23, 24]. In our work, we base GPP on the last-mentioned approach due to the outdoor requirement of our future applications.

Local Path Planning (LPP) uses the vehicle sensors, such as LiDAR and/or cameras, to understand the local environment. In this way, LPP can re-plan the path as function of the obstacles closer to the vehicle. The LPP can be divided into static LPP [25, 26], which can detect only static objects (but not necessarily persistent), and dynamic LPP [27, 28], which tracks dynamic objects and consider their trajectories to re-plan the path. In the literature, there are many works based on classical algorithms for obtaining local paths, such as the Artificial Potential Field method [29], Fuzzy Logic Algorithm [30, 31], Simulated Annealing Algorithm [32], a hybrid method combined with a genetic algorithm [33], and the particle algorithm [34], where the authors avoid the disadvantage that the solution is locally optimal. Another extended LPP is the optimization sample-based

methods [35]. In this case, the local environment is represented as a cost map sampled, usually as a grid map. Then, the local path that minimizes the cost in the map is searched using algorithms such as A* [36] or RRT* [37]. On the one hand, the flaw in these approaches is that both the generation of local maps and the optimization process could be expensive in time-consuming terms. On the other hand, the cost maps are usually informative around obstacles, but they don't usually have enough information about "where-is" the center of trafficable regions. For that reason, we focus our LPP on a time-efficient version of the last-mentioned optimization sample-based methods by avoiding obstacles through areas always at the center of trafficable regions.

Additionally, in the last years, there have been many works focused on learning-based path planning methods [38]. The end-to-end self-driving methods compress the whole process of planning-control in one step based on a Convolutional Neural Network (CNN) [39, 40], where the sensor data is the input of the network and where the control actions are the output. Another learning-based approach is the Reinforcement Learning (RL) [41, 42], where the learning process occurs during vehicle navigation. In these cases, the time-consuming is also a challenging issue.

In this paper, we present a complete autonomous navigation pipeline. This work is in the context of a real application for a project that addresses the problem of garbage "pick and place" in the University of Alicante campus using UGV. For this reason, we assume an unstructured outdoor environment for our application, where the localization is GPS-IMU based, in a global frame coordinates system [43]. Given these assumptions, we don't consider grid maps appropriate for GPP in our application. Instead, we use road network information obtained directly from OpenStreetMap (OSM). This map-less GPP frees us from the limitation of the work area size, and it would allow us to explore areas not previously navigated. In the LPP layer, we use a novel Naive-Valley-Path method (NVP) to generate a local path avoiding obstacles in the road in real-time. NVP is in the context of optimization sample-based methods. This approach uses a naive representation of a cost map. Also, it implements a naive optimization exploiting the concept of "valley" areas in the cost map, i.e., the ones always away from obstacles that provides information about the center of trafficable regions. Due to the low execution time of our NVP algorithm, we can avoid dynamic obstacles such as vehicles and pedestrians, as we demonstrate experimentally. In this case, we cannot consider this method completely dynamic because we do not use tracking to predict obstacles trajec-

tories. So, considering that, we can define our approach as "semi-dynamic".

To summarize, the main contributions are the following:

- A complete outdoor autonomous navigation system in unstructured environments, based on GPS-IMU fusion localization, OSM for GPP, and a naive cost-map-sampled-based LPP for obstacle avoidance using LiDAR measurements.
- A novel real-time obstacle avoidance method called Naive-Valley-Path (NVP) which infers a naive cost map represented as concentric circles around the robot to obtain the optimal local path using points in "valley" areas. This method provides two main advantages against state-of-the-art ones: low time consumption and navigation always following the center of trafficable areas.
- Test and comparison with other state-of-the-art OSM-based autonomous navigation [36] using our own developed research platform BLUE [44] and our navigation framework [45].

The rest of the paper is organized as follows: In Section 2, we present an overview of the complete Path Planning method proposed. Then, local Path Planning and Global Path Planning modules are described in Sections 3 and 4, respectively. Next, in Section 5, we show the experimental results obtained using our own real robot BLUE. Finally, in Section 6, we present the main conclusions obtained from this work and possible future works.

2. Proposed Approach Architecture

In Fig. 1, we show the proposed approach, which is divided into different modules. The path planning is organized hierarchically. At the top-level, we compute the GPP that receives a graph obtained from the online application OSM, the final global goal provided by the user, and the pose obtained from the localization module. In this work, we assume that we have a georeferenced global localization. This is required to use the environment representation directly from OSM, which provides geolocalized information about roads and intersections. The GPP infers the best path through the graph using the A* algorithm, and it gives as output a local goal, which is the nearest node of the calculated path.

This goal is an input for the LPP module. Moreover, the LPP receives as inputs the vehicle's localization and

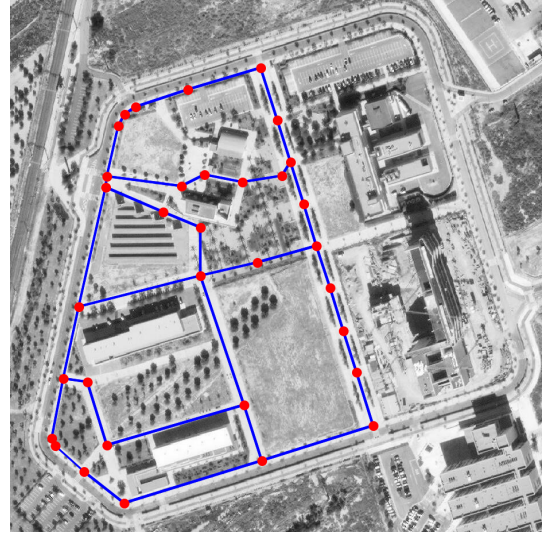


Figure 2: Example of Graph used in the GPP module, in this case, extracted from the Scientific Park area in the University of Alicante. The red points describe the georeferenced position of nodes, while the blue lines represent the links that indicate a trafficable connection between nodes. We can extract the graph directly from current OSM data or create it manually in the JOSM application.

3D LiDAR scans from the sensor. We divided the LPP hierarchically into three layers. In the "Free-space" calculation layer, we remove ground points and the points above the upper part of the vehicle. Then, we consider the rest of the points as obstacles that we use as borders of a free-space representation 2D map. In the Naive-Valley-Path NVP layer, we use a naive cost map representation in the free-space map to infer an optimal path exploiting the concept of "valley" areas. Finally, we evaluate the possible actions, among ones without collision risk, that minimize the error between the vehicle pose and the local path.

In Section 3 and Section 4, we explain in more detail each module of the proposed approach.

3. Global Path Planning

At the Global Path Planning level, we need a representation of the environment. This representation can contain trees, buildings, traffic signals, roads, intersections, etc. If and only if we think at the GPP level, we can consider this representation of the environment as persistent static. Under this assumption, we decided to use the environment information from online applications such as OpenStreetMaps (OSM), which contains georeferenced persistent static elements. With this representation, we avoid the use of complex maps that usually give some problems, such as memory limitation,

hard inference, and global inconsistencies produced by accumulated drifts.

We represent the environment as a graph, in which each node is a georeferenced point in a trafficable area, and each link indicates that two points are connected through a passable road. In Fig. 2, we show an example of the graph plotted over the OSM map. We can obtain the graph representation directly by OSM down-sampling the paths to lighten the process. Also, we can add nodes manually to areas that we know are trafficable using the software of OSM called JOSM. Given graph \mathcal{G} , we find the best path between the nearest node to the vehicle's pose and the node nearest to the global goal provided by the user. For this search, we use the A* algorithm. Once the path has been obtained, we store the pose of the nodes in a buffer. Finally, we send each node sequentially as a local goal to the LPP module as they are being reached. We consider a local goal reached when the Mahalanobis Distance (MD) [46] is less than a certain configurable threshold. Using this probabilistic distance, we can evaluate if a goal is reached depending on the covariance in the localization system. In this way, we can prevent severe deviation from reaching goals in case of considerable noisy localization.

4. Local Path Planning

In this section, we describe the Local Path Planning module, which is divided hierarchically into three levels. This module aims to infer the final control actions to send to the vehicle's actuators. Also, in this process, we use the LiDAR sensor to avoid possible obstacles in the local goal-reaching.

4.1. Obstacles and Free-space Calculation

We consider as obstacles the points in a LiDAR point cloud that are not part of the surface on which the vehicle circulates, i.e., the ones that are representing objects above the ground, or even points under the ground, such as descending steps. Besides, we consider obstacles only the points that are under the upper part of the vehicle, which is the collision risk fringe.

Given this definition, we need to detect the ground points to consider obstacles to the rest. In large part of the scenarios, we observed the ground surface is usually flat. Hence, we make a plane assumption using the LiDAR point cloud \mathcal{P} for a nonlinear Least-Squares optimization (based on [47]) to find the optimal ground plane parameters (1) that minimize the accumulated point-to-plane error for all points $\mathbf{p} \in \mathcal{P}$:

$$\mathbf{pl}^* = \arg \min_{\mathbf{pl}} \sum_{\mathbf{p} \in \mathcal{P}} \rho(\|\mathbf{e}(\mathbf{pl}, \mathbf{p})\|^2) \quad (1)$$

Where $\mathbf{e}(\mathbf{pl}, \mathbf{p})$ denotes the distance vector between \mathbf{p} and its plane projection point. The loss function ρ is chosen to be the Cauchy loss with a small scale to be robust against outliers. We then remove all points from the point set with a distance below a threshold to the \mathbf{pl}^* plane. To consider possible slope changes in the terrain, we apply this threshold proportionally to the distance to the sensor center. Finally, we displace the plane in the z axis to the upper part of the vehicle, and we then remove the points over this second plane. The points that remain in \mathcal{P} after this process are what we consider obstacles in a new point cloud \mathcal{P}^o . In Fig. 3 a), we show an example of \mathcal{P}^o projected in a 2D plane.

Starting from \mathcal{P}^o , we build a 2D representation of the free space. We define free space as the area inside a polygon where the contours are obstacle points. To build the polygon, first, we represent \mathcal{P}^o as a grid using a spherical representation. The rows and columns in this grid represent the elevation and azimuth angles, respectively, and the value in each cell is the range value. The cells with no point information have an empty value. Then, we sweep the columns of the grid. If the column contains points, we choose the one with the lowest range value, and we project it in a 2D cartesian representation (xy). The points selected are the ones that form the free-space polygon. In Fig. 3 b), we show an example of free-space map.

4.2. Valley-Path Calculation

Once we know the free space around the vehicle, we need to determine a path in that space to reach the local goal. For this, we use a cost representation of free space. We consider the local goal as an attractor p_a and the nearest obstacle point as a repulsor p_r . Then, for each discrete point p_{ij} in the free space, we obtain the cost as follows:

$$f_{ij} = \frac{w_r}{(p_{ij} - p_r)^{\gamma_r}} - \frac{w_a}{(p_{ij} - p_a)^{\gamma_a}} \quad (2)$$

Where w_a and w_r are the weight of the attractive potential and the repulsive potential, respectively. And where γ_a and γ_r are the parameters to control the decay of the potential with respect to the distance. In Fig. 3 c), we show an example of our cost map representation for single LiDAR scan. We consider that we always want to navigate through the areas furthest from obstacles. Then, focusing on yellow areas in Fig. 3 c), we can observe that these areas are ones around local minimal. We name these areas as "valleys" from now on.

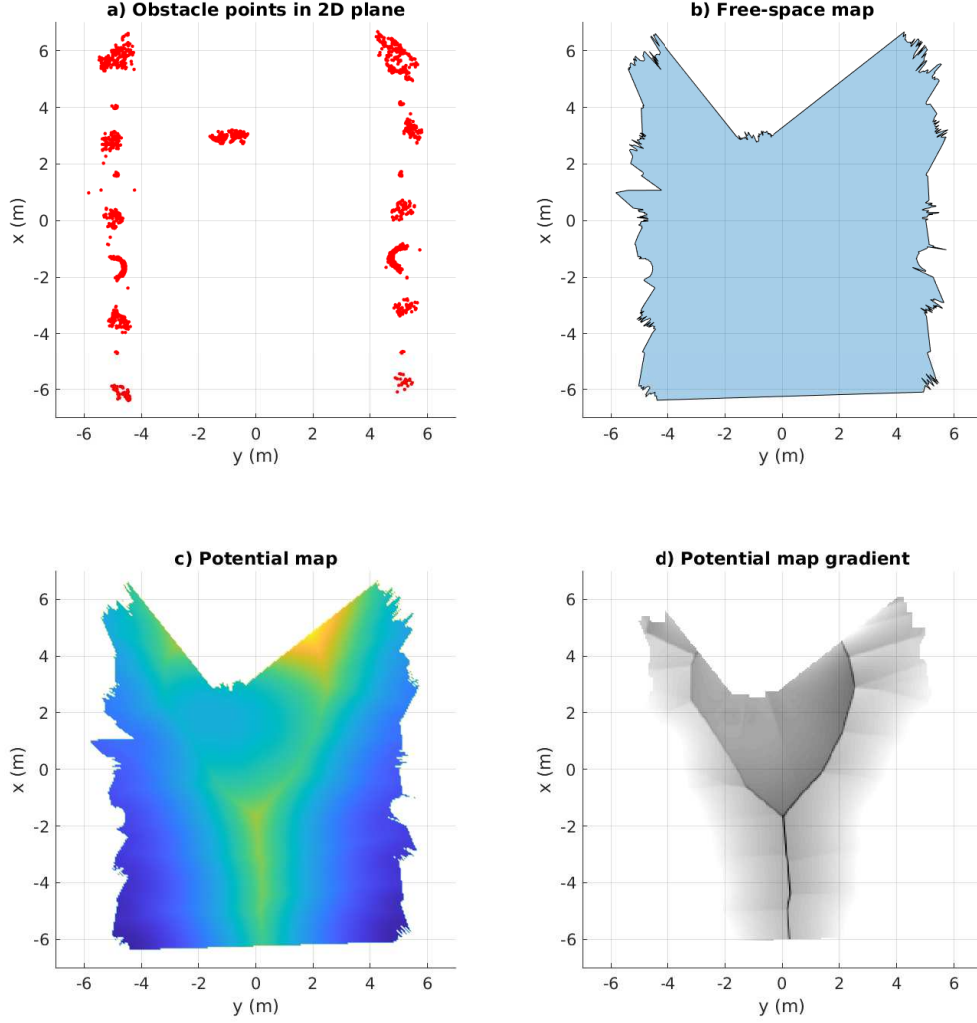


Figure 3: Different 2D representation of LiDAR information for Valley-Path calculation: a) Projection in a 2D plane of obstacles point cloud \mathcal{P}^o . b) Free-space map, where the blue area represents the space free of obstacles. c) Cost map defined in (2). d) Inverted representation of the gradient magnitude of c), which shows clear possible paths in the valley areas.

To segment the valleys in the map, we assume that the values of the magnitude of the gradient at point f_{ij} close to zero can be considered a point in a valley. Then, each point that satisfies (3) is labeled as a valley.

$$|\nabla f_{ij}| < \xi \quad (3)$$

Where ξ is a configurable threshold. Fig. 3 d) shows an example of a segmented valley. In the example, the darkest points mark the lowest magnitude of gradient points. We can see that this representation define clearly

possible Valley-Paths.

To infer a Valley-Path between the robot pose and the global minimum in the map, we could use the gradient cost map for an optimization process such as A* or Dijkstra [48]. However, this approach has the flaw of being excessively time-consuming in computational terms. For this reason, we develop a "naive" version of this Valley-Path calculation that we explain in Section 4.3.

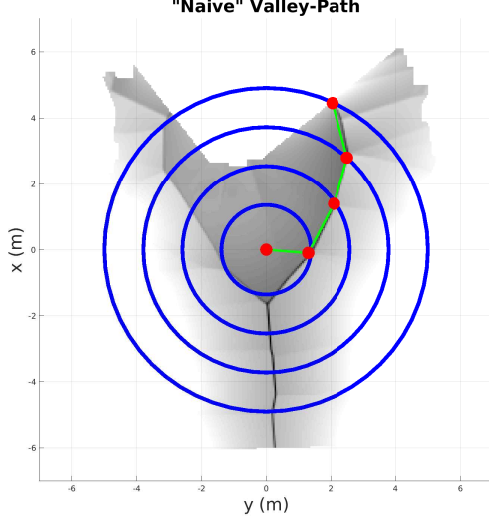


Figure 4: The Naive-Valley-Path (NVP) Calculation. The red points are the ones that form the local path. The green connections describe the **naive assumption** and define the angle of the points. For the sake of clarity, this representation shows the NVP superpose with non-naive representation.

4.3. Naive Version of the Valley-Path Calculation

Given a circle around the sensor pose, for each polar coordinate (r, φ_i) we can apply the expression (4), which is the 1D version of (2).

$$f_i = \frac{w_r}{(p_i - p_r)^{\gamma_r}} - \frac{w_a}{(p_i - p_a)^{\gamma_a}} \quad (4)$$

If we represent this 1-dimensional signal as a magnitude of the gradient, we can label as valley points the ones that satisfy (3). We can do the same process in inner concentric circles. In this way, we can make the following **naive assumption**: given a valley point $p_i^{c_1}$ in a circle c_1 , and given the nearest valley point $p_n^{c_2}$ in an inner circle c_2 , the line that connects $p_i^{c_1}$ with $p_n^{c_2}$ is considered part of a path in the same valley. The subscript n means the index of the nearest valley point.

Under this assumption, given a set of N circles (c_0, c_1, \dots, c_N) , we can define the Naive-Valley-Path (NVP) as a set of join points $(p_n^{c_0}, p_n^{c_1}, \dots, p_n^{c_N})$ in which each element is connected with the nearest previous one. The first point $p_n^{c_0}$ is the valley point in the external circle nearest to the local goal p_a . As N increases, the time consumption also increases, and the result can converge to the non-naive version of the Valley-Path calculation. The process described in this section is executed each time a LiDAR scan is received, i.e., the local path is recalculated in each iteration. In Fig. 4 we show an

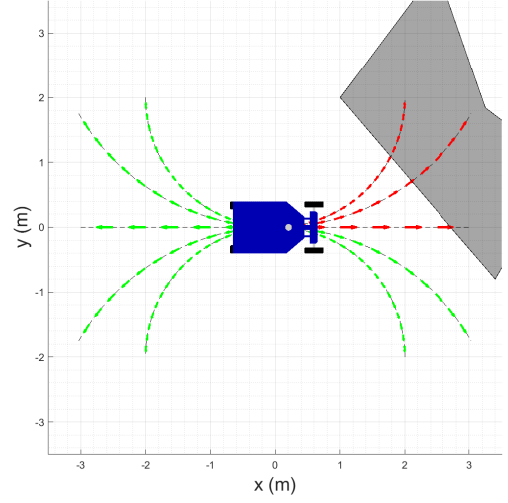


Figure 5: The arcs represent the possible trajectories of control actions u_i . The red ones are the collision-risk trajectories, and their corresponding control actions are discarded. In contrast, the green ones are collision-free.

example of NVP and the circles used for the inference. To more clearly show how NVP follows the valley areas, in Fig. 4 we superpose it to the original non-naive representation.

4.4. Control Actions Calculation

Finally, in the lower-level layer, given a local path, we obtain the control actions $u = (v, \alpha)$ that are the output of the LPP module. v is the linear absolute velocity of the vehicle, and α is the steering position. For this, we compute a prediction of trajectories for any possible α at the front and rear directions (Fig. 5). Given a sampled i -th trajectories and the size of the vehicle, we evaluate the collision risk for each one. If some part of the vehicle (with an added security margin) is out from the free-space map at any point of a i -th trajectory, the whole trajectory is considered to be at risk of collision, and it associated α_i is discarded as possible variable for the control action. Fig. 5 shows an example of estimated trajectories where the red ones are labeled as collision-risk.

Once we have the collision-free trajectories (green ones in Fig. 5), we evaluate the error between each j -th pose in a i -th trajectory x_{ij} and each k -th pose p_k in the complete local path. We compute error as follows:

$$e_{ijk} = c^p \left(|x_{ij}^p - p_k^p| \right) + c^o \left(x_{ij}^o - p_k^o \right) \quad (5)$$

And we minimizes it as:



Figure 6: Our UGV *BLUE: roBot for Localization in Unstructured Environments* [44].

$$i^* = \min_{\forall i} \left(\sum_j \sum_k e_{ijk} \right) \quad (6)$$

Where superscript and subscript p and o mean position and orientation, respectively, and where c^p and c^o are configurable constants to relate the different magnitudes. The result i^* is the index for the control action variable α_i . The variable v of the control action is computed as follows:

$$v = v_{max} - |\alpha_i| \frac{v_{max} - v_{min}}{\alpha_{max}} \quad (7)$$

Where v_{max} , v_{min} , and α_{max} , are configurable parameters that depends on the vehicle's characteristics. In case of no collision-free trajectories, control action variables are $\alpha = 0$ and $v = 0$.

5. Evaluation

We evaluated the autonomous navigation system presented in this paper in our research platform *BLUE: roBot for Localization in Unstructured Environments* [44] (Fig. 6). This robot includes actuators for speed and steering, traction and steering encoders, IMU, GPS Ublox M8P, camera RGBD Intel Realsense D435, and LiDAR 3D Velodyne VLP16. All them integrated into *Robot Operating System* (ROS). The developed software is included in the framework for fast experimental

testing presented in [45]. We use a fusion of wheel-encoders, IMU, and GPS as a localization system that provides localization in global coordinates. The error of this system is subject to the error in GPS, which in our experimental sessions reaches peaks until 15 meters of variance in the xy plane. Our path planning modules demonstrated robustness against these localization measurement errors.

We carried out the experiments in the Scientific Park at the University of Alicante. This area contains parking lots and pedestrian walkable areas with trees, benches, and curbs (Fig. 2). We chose this scenario for the experiments because it is where the "pick and place" application commented in the introduction is projected.

In Section 5.1, we demonstrate the main advantage of the OSM-based GPP module, which is the possibility of global goal reaching in an extensive area where grid-based approaches fail. Also, in Section 5.1, we evaluate one of our LPP module (NVP) advantages, which is the navigation in the center of the road, compared to another state-of-the-art one [36]. In Section 5.2, we evaluate the presented NVP for obstacle avoidance and compare it with the same previous commented method, demonstrating how our system recovers better the center of the road after obstacle avoidance. Finally, in Section 5.3, we evaluate the time consumption, which is the other main advantage of our NVP, by comparing with [36].

5.1. Trajectory Evaluation in Global Goal-Reaching

We test the global goal-reaching for our system using the graph shown in Fig. 2. Due to this area being newly constructed, there is no information in OSM concerning trafficable paths. Hence, we created the road network by hand using the JOSM application. Given this graph and the current localization, we send a global goal by hand at a certain point of the network and record the vehicle's autonomous trajectory during the process. Once the goal is reached, we repeat the global goal sending sequentially to cover most of the area of the experiment. In Fig. 7, we show the results after doing the process described above, where we mark the start of each path and its sent global goal.

It is worth noting that the graph connections are only for the GPP layer and don't describe precisely the road layout. For this reason, we cannot use the black lines in Fig. 7 as reference for trajectory evaluation. The task of driving the vehicle through the center of the road falls on the LPP layer. Then, to evaluate the system quantitatively and compare it with another state-of-the-art one, we drove manually the same paths through the center of the road to use them as ground truth.

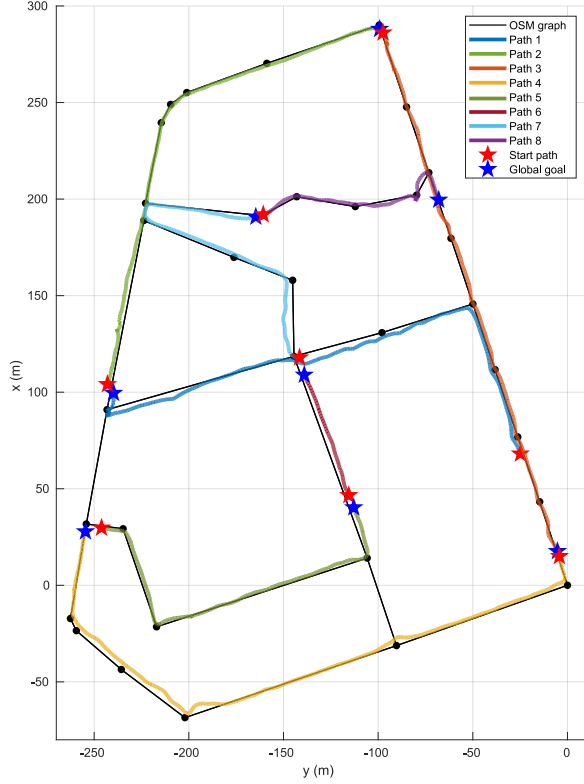


Figure 7: Evaluation of global goal-reaching. The red marks indicate the vehicle location when a goal was sent, and the blue marks indicate the sent goal locations.

Given the ground truth, it was impossible to compare our system with others that use grid maps for GPP. We had problems generating this kind of map in this extensive and highly unstructured environment, which demonstrates the improvement of our GPP module against a vast part of state-of-the-art works. Hence, we compared our approach with another OSM-based autonomous navigation system [36]. The LPP layer on [36] uses a cost map constructed from road edge detection from the camera and a classic A* algorithm for optimization. In Table 1, we show the comparison of error measures against ground truth for both systems. We can see that our method follows better the center of the road in this environment.

Table 1: Deviation from the center of the road.

Deviation	NVP-based	A*-based [36]
Average error (m)	0.24	0.32
Max error (m)	0.72	0.98

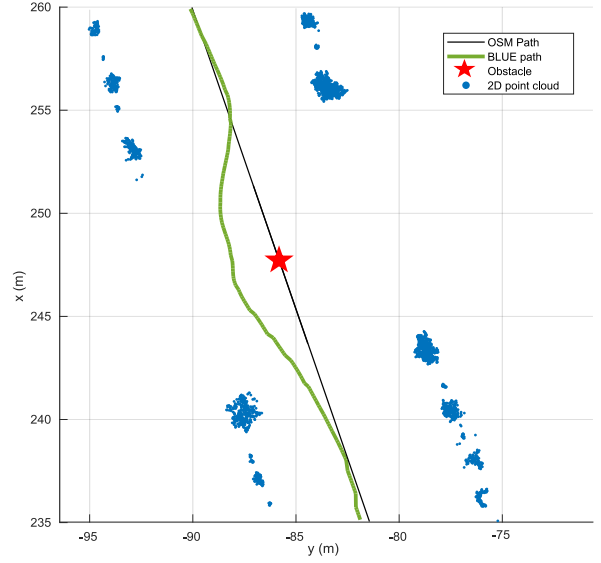


Figure 8: Our system behavior in the face of a static obstacle in the center of the road.

5.2. Obstacle-Avoidance Evaluation

In the previous section, we evaluated the whole trajectory, which is a task that combines GPP and LPP. However, this trajectory evaluation is for an application in a university campus environment, and, hence, we need to evaluate the behavior of our LPP in the face of unforeseen obstacles.

In Fig. 8, we show our system behavior in the face of a static obstacle in the center of the road. In this case, the black line can serve as a reference, due to, in this case, the road is straight. In order to test how the system recovers the center of the road after obstacle avoidance, in Fig. 9, we show the absolute error evolution against the black line in Fig. 8 and compare it with the error evolution in the same obstacle avoidance for [36]. We can see that our NVP method can recover the center of the road faster than the tested [36] method.

How our system avoids obstacles depends on the parameter γ_r described in (4), due to it defining the decay of our potential cost map (Fig. 3 c)). When $\gamma_r > 0$, while γ_r increases, the decay in the cost map increases and the trajectory could pass closer to the obstacles. In Fig. 10, we show an example of this behavior for three different gamma configurations in the same scenario as the previous experiment. The parameter γ_a models the behavior of obstacle avoidance only in the area close to the local goal. For this reason, we configure it constant for the example.

We also evaluate obstacle avoidance for dynamic obstacles such as pedestrians and vehicles qualitatively.

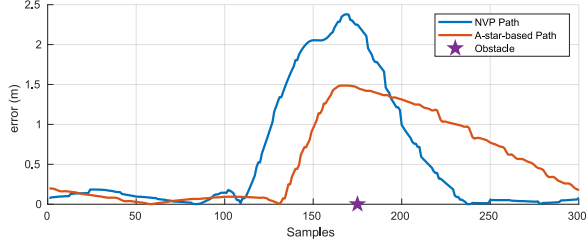


Figure 9: Absolute error evolution against the black line in Fig. 8 of our system comparing with the error evolution in the same obstacle avoidance for [36].

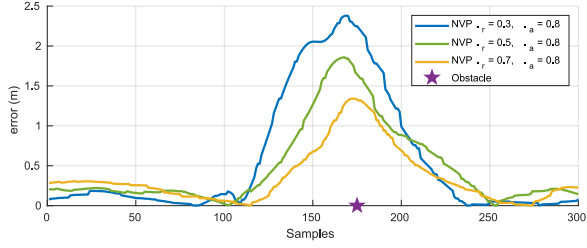


Figure 10: Example of different error evolution for different γ_r parameter configurations in our NVP potential cost map (4).

Fig. 11 shows an image sequence of repeated pedestrian avoidance, where the time evolution is from left to right. We enumerate these images from 1 to 5. In image 1, we can see a pedestrian running to cross the vehicle's trajectory. The vehicle rectifies his local path, but the pedestrian stops just in the front of the vehicle (image 2). In the transition from image 2 to image 3, the vehicle maneuvers, first in the rear direction and after in the front direction, to avoid the pedestrian, but then the pedestrian stops in front of the vehicle again (image 4). Finally, in image 5, the vehicle avoids the pedestrian and continues the travel to reach the goal.

In Fig. 12, we show another example of obstacle avoidance: a car in a parking lot. In this case, the vehicle follows a straight trajectory, but a car drive to cross this trajectory. However, due to the NVP Local Path Planning module, the vehicle recalculates the path to avoid this dynamic obstacle, as shown in the sequence of Fig. 12.

5.3. Time-Consuming Evaluation

The other advantage of our NVP path planning method is that it is speedy compared to other optimization approaches. To compare the time-consuming, we measured the sample time and total time of the NVP experiment shown in Fig. 11, where the number of circles (Section 4.3) is configured $N = 4$ (NVP4). Also, we

repeat this process by configuring $N = 8$ (NVP8). Finally, we repeat the process for the A*-based approach [36]. We performed the time measurement for this experiment by running the algorithms as C++ compiled codes on an i7-7700HQ CPU with 16 GB of RAM.

Table 2: Comparison of time-consuming.

Time	NVP4	NVP8	[36]
Average s. time (ms)	19.8	32.8	92.7
Max s. time (ms)	24.7	38.5	122.8
Total time (s)	36	38	53

We can see in Table 2 that our approach can complete the scenario shown in Fig. 11 faster than the A*-based one. In the case of [36], we can use only 10 Hz sensors. In contrast, our NVP could implement sensors even with 40/50 Hz of frequency, allowing faster response in the face of dynamic obstacles.

6. Conclusions And Future Works

In this paper, we have presented a complete autonomous navigation pipeline for Unmanned Ground Vehicles (UGV) in unstructured outdoor environments. The path planning module is the main contribution divided hierarchically into Global Path Planning and Local Path Planning. The first module allows planning paths at a high level without an exhaustive environment representation, freeing the application of area size constraints. The LPP module allows, in a fast way, obstacle avoidance in the path using the concept of Valley-Paths, which are the local paths that follow the areas away from obstacles. This allows always navigating through the center of trafficable regions. We demonstrate the potential of the method experimentally to reach global goals through the center of the road. Also, we show how our NVP based LPP achieves fast and robust obstacle avoidance even in dynamic cases, such as cars and pedestrians, and how it recovers the center of the road after avoidance.

As future works, we plan to use an online interface with JOSM to make a dynamic graph for the GPP. In this way, we could navigate in an exploration mode into completely unknown areas. Also, we plan to use more sophisticated perception techniques, such a Convolutional Neural Networks (CNN), to classify obstacles in the environment.



Figure 11: **Obstacle avoidance experiments:** Example of pedestrian avoidance in an image sequence. A pedestrian crosses the vehicle trajectory twice (images 2 and 4 from left to right). In both cases, the vehicle avoids this dynamic obstacle by doing rear maneuvering.



Figure 12: **Obstacle avoidance experiments:** Example of car avoidance in an image sequence. The vehicle circulates in a straight-line way and modifies its trajectory when a car crosses its path.

References

- [1] B. Ichter, J. Harrison, M. Pavone, Learning sampling distributions for robot motion planning, in: 2018 IEEE International Conference on Robotics and Automation (ICRA), IEEE, 2018, pp. 7087–7094.
- [2] A. Toriz Palacios, A. Sánchez López, Sobre la mejora esperada de la estimación de la odometría en exploración integrada, *Revista Iberoamericana de Automática e Informática industrial* 17 (2) (2020) 229–238.
- [3] J.-R. Xue, J.-W. Fang, P. Zhang, A survey of scene understanding by event reasoning in autonomous driving, *International Journal of Automation and Computing* 15 (3) (2018) 249–266.
- [4] L. Zhu, X. Cheng, F.-G. Yuan, A 3d collision avoidance strategy for uav with physical constraints, *Measurement* 77 (2016) 40–49.
- [5] S. G. Tzafestas, Mobile robot control and navigation: A global overview, *Journal of Intelligent & Robotic Systems* 91 (1) (2018) 35–58.
- [6] K. Cai, C. Wang, J. Cheng, C. W. De Silva, M. Q.-H. Meng, Mobile robot path planning in dynamic environments: A survey, *arXiv preprint arXiv:2006.14195* (2020).
- [7] J. Guzzi, R. O. Chavez-Garcia, M. Nava, L. M. Gambardella, A. Giusti, Path planning with local motion estimations, *IEEE Robotics and Automation Letters* 5 (2) (2020) 2586–2593.
- [8] D. Kularatne, S. Bhattacharya, M. A. Hsieh, Optimal path planning in time-varying flows using adaptive discretization, *IEEE Robotics and Automation Letters* 3 (1) (2017) 458–465.
- [9] P. C. Chen, Y. K. Hwang, Sandros: a dynamic graph search algorithm for motion planning, *IEEE Transactions on Robotics and Automation* 14 (3) (1998) 390–403.
- [10] L. Schmid, M. Pantic, R. Khanna, L. Ott, R. Siegwart, J. Nieto, An efficient sampling-based method for online informative path planning in unknown environments, *IEEE Robotics and Automation Letters* 5 (2) (2020) 1500–1507.
- [11] S. Karaman, E. Frazzoli, Sampling-based algorithms for optimal motion planning, *The international journal of robotics research* 30 (7) (2011) 846–894.
- [12] T. Chen, A simulative bionic intelligent optimization algorithm: artificial searching swarm algorithm and its performance analysis, in: 2009 International Joint Conference on Computational Sciences and Optimization, Vol. 2, IEEE, 2009, pp. 864–866.
- [13] S. Broumi, A. Bakal, M. Talea, F. Smarandache, L. Vladareanu, Applying dijkstra algorithm for solving neutrosophic shortest path problem, in: 2016 International conference on advanced mechatronic systems (ICAMEchS), IEEE, 2016, pp. 412–416.
- [14] F. Duchoñ, A. Babinec, M. Kajan, P. Beño, M. Florek, T. Fico, L. Jurišica, Path planning with modified a star algorithm for a mobile robot, *Procedia Engineering* 96 (2014) 59–69.
- [15] M. Guo, K. H. Johansson, D. V. Dimarogonas, Revising motion planning under linear temporal logic specifications in partially known workspaces, in: 2013 IEEE International Conference on Robotics and Automation, IEEE, 2013, pp. 5025–5032.
- [16] J. Yu, S. M. LaValle, Planning optimal paths for multiple robots on graphs, in: 2013 IEEE International Conference on Robotics and Automation, IEEE, 2013, pp. 3612–3617.
- [17] X. Dai, S. Long, Z. Zhang, D. Gong, Mobile robot path planning based on ant colony algorithm with a* heuristic method, *Frontiers in neurorobotics* 13 (2019) 15.
- [18] S. Li, W. Su, R. Huang, S. Zhang, Mobile robot navigation algorithm based on ant colony algorithm with a* heuristic method, in: 2020 4th International Conference on Robotics and Automation Sciences (ICRAS), IEEE, 2020, pp. 28–33.
- [19] E. Tsardoulis, A. Iliakopoulou, A. Kargakos, L. Petrou, A review of global path planning methods for occupancy grid maps regardless of obstacle density, *Journal of Intelligent & Robotic Systems* 84 (1) (2016) 829–858.
- [20] Y. Chen, G. Bai, Y. Zhan, X. Hu, J. Liu, Path planning and obstacle avoiding of the usv based on improved aco-apf hybrid algorithm with adaptive early-warning, *IEEE Access* (2021).
- [21] J. Laconte, A. Kasmí, F. Pomerleau, R. Chapuis, L. Malaterre, C. Debain, R. Aufrère, Lambda-field: A continuous counterpart of the bayesian occupancy grid for risk assessment and safe navigation, *arXiv preprint arXiv:2011.08045* (2020).
- [22] V.-D. Hoang, D. C. Hernández, J. Hariyono, K.-H. Jo, Global path planning for unmanned ground vehicle based on road map images, in: 2014 7th International Conference on Human System Interactions (HSI), IEEE, 2014, pp. 82–87.
- [23] A. Artuñedo, J. Godoy, J. Villagra, A decision-making architecture for automated driving without detailed prior maps, in:

- 2019 IEEE Intelligent Vehicles Symposium (IV), IEEE, 2019, pp. 1645–1652.
- [24] B. Suger, W. Burgard, Global outer-urban navigation with open-streetmap, in: 2017 IEEE International Conference on Robotics and Automation (ICRA), IEEE, 2017, pp. 1417–1422.
 - [25] Z. B. Garip, G. Atali, D. Karayel, S. S. Ozkan, Path planning for multiple mobile robots in static environment using hybrid algorithm, in: 2018 2nd International Symposium on Multidisciplinary Studies and Innovative Technologies (ISMSIT), IEEE, 2018, pp. 1–4.
 - [26] T. XiangRong, Z. Yukun, J. XinXin, Improved a-star algorithm for robot path planning in static environment, in: Journal of Physics: Conference Series, Vol. 1792, IOP Publishing, 2021, p. 012067.
 - [27] J. Ji, A. Khajepour, W. W. Melek, Y. Huang, Path planning and tracking for vehicle collision avoidance based on model predictive control with multiconstraints, IEEE Transactions on Vehicular Technology 66 (2) (2016) 952–964.
 - [28] W. Yaonan, Y. Yimin, Y. Xiaofang, Z. Yi, Z. Yuanli, Y. Feng, T. Lei, Autonomous mobile robot navigation system designed in dynamic environment based on transferable belief model, Measurement 44 (8) (2011) 1389–1405.
 - [29] A. Le Gougec, A. Kemeny, A. Berthoz, F. Merienne, Artificial potential field simulation framework for semi-autonomous car conception, Science Arts and Metiers (2017).
 - [30] A. Bakdi, A. Hentout, H. Boutami, A. Maoudj, O. Hachour, B. Bouzouia, Optimal path planning and execution for mobile robots using genetic algorithm and adaptive fuzzy-logic control, Robotics and Autonomous Systems 89 (2017) 95–109.
 - [31] A. Ebrahimnejad, M. Tavana, H. Alrezaamiri, A novel artificial bee colony algorithm for shortest path problems with fuzzy arc weights, Measurement 93 (2016) 48–56.
 - [32] T. Turker, O. K. Sahingoz, G. Yilmaz, 2d path planning for uavs in radar threatening environment using simulated annealing algorithm, in: 2015 International Conference on Unmanned Aircraft Systems (ICUAS), IEEE, 2015, pp. 56–61.
 - [33] P. Paulo, F. Branco, J. de Brito, A. Silva, Buildingslife—the use of genetic algorithms for maintenance plan optimization, Journal of cleaner production 121 (2016) 84–98.
 - [34] M. Petrović, N. Vuković, M. Mitić, Z. Miljković, Integration of process planning and scheduling using chaotic particle swarm optimization algorithm, Expert systems with Applications 64 (2016) 569–588.
 - [35] J. D. Gammell, M. P. Strub, Asymptotically optimal sampling-based motion planning methods, Annual Review of Control, Robotics, and Autonomous Systems 4 (2021) 295–318.
 - [36] J. Li, H. Qin, J. Wang, J. Li, Openstreetmap-based autonomous navigation for the four wheel-legged robot via 3d-lidar and ccd camera, IEEE Transactions on Industrial Electronics (2021).
 - [37] W. Chi, C. Wang, J. Wang, M. Q.-H. Meng, Risk-dtrrt-based optimal motion planning algorithm for mobile robots, IEEE Transactions on Automation Science and Engineering 16 (3) (2018) 1271–1288.
 - [38] J. Cheng, H. Cheng, M. Q.-H. Meng, H. Zhang, Autonomous navigation by mobile robots in human environments: A survey, in: 2018 IEEE International Conference on Robotics and Biomimetics (ROBIO), IEEE, 2018, pp. 1981–1986.
 - [39] M. Bojarski, D. Del Testa, D. Dworakowski, B. Firner, B. Flepp, P. Goyal, L. D. Jackel, M. Monfort, U. Muller, J. Zhang, et al., End to end learning for self-driving cars, arXiv preprint arXiv:1604.07316 (2016).
 - [40] P. Cai, S. Wang, Y. Sun, M. Liu, Probabilistic end-to-end vehicle navigation in complex dynamic environments with multimodal sensor fusion, IEEE Robotics and Automation Letters 5 (3) (2020) 4218–4224.
 - [41] X. Pan, Y. You, Z. Wang, C. Lu, Virtual to real reinforcement learning for autonomous driving, arXiv preprint arXiv:1704.03952 (2017).
 - [42] B. Wang, Z. Liu, Q. Li, A. Prorok, Mobile robot path planning in dynamic environments through globally guided reinforcement learning, IEEE Robotics and Automation Letters 5 (4) (2020) 6932–6939.
 - [43] M. M. Atia, S. L. Waslander, Map-aided adaptive gnss/imu sensor fusion scheme for robust urban navigation, Measurement 131 (2019) 615–627.
 - [44] I. del Pino, M. A. Munoz-Banon, S. Cova-Rocamora, M. A. Contreras, F. A. Candelas, F. Torres, Deeper in blue, Journal of Intelligent & Robotic Systems 98 (1) (2020) 207–225.
 - [45] M. Á. Muñoz-Bañón, I. del Pino, F. A. Candelas, F. Torres, Framework for fast experimental testing of autonomous navigation algorithms, Applied Sciences 9 (10) (2019) 1997.
 - [46] R. De Maesschalck, D. Jouan-Rimbaud, D. L. Massart, The mahalanobis distance, Chemometrics and intelligent laboratory systems 50 (1) (2000) 1–18.
 - [47] S. Wirges, C. Stiller, F. Hartenbach, Evidential occupancy grid map augmentation using deep learning, in: 2018 IEEE intelligent vehicles symposium (IV), IEEE, 2018, pp. 668–673.
 - [48] M. K. Ardakani, M. Tavana, A decremental approach with the a-star algorithm for speeding-up the optimization process in dynamic shortest path problems, Measurement 60 (2015) 299–307.